Biochemistry

Article

Cite This: *Biochemistry* 2018, 57, 978–990

pubs.acs.org/biochemistry

Cluster-Dependent Charge-Transfer Dynamics in Iron–Sulfur Proteins

Ziliang Mao,[†] Shu-Hao Liou,[†,⊥] Nimesh Khadka,[§,#] Francis E. Jenney, Jr.,[‡] David B. Goodin,[†] Lance C. Seefeldt,[§] Michael W. W. Adams,[∥] Stephen P. Cramer,*[,†] and Delmar S. Larsen*[,†]

[†]Department of Chemistry, University of California at Davis, One Shields Avenue, Davis, California 95616, United States

[‡]Georgia Campus, Philadelphia College of Osteopathic Medicine, Suwanee, Georgia 30024, United States

[§]Department of Chemistry and Biochemistry, Utah State University, 0300 Old Main Hill, Logan, Utah 84322, United States

[∥]Department of Biochemistry, The University of Georgia, Athens, Georgia 30602, United States

Supporting Information

ABSTRACT: Photoinduced charge-transfer dynamics and the influence of cluster size on the dynamics were investigated using five iron–sulfur clusters: the 1Fe–4S cluster in *Pyrococcus furiosus* rubredoxin, the 2Fe–2S cluster in *Pseudomonas putida* putidaredoxin, the 4Fe–4S cluster in nitrogenase iron protein, and the 8Fe–7S P-cluster and the 7Fe–9S–1Mo FeMo cofactor in nitrogenase MoFe protein. Laser excitation promotes the iron–sulfur clusters to excited electronic states that relax to lower states. The electronic relaxation lifetimes of the 1Fe–4S, 8Fe–7S, and 7Fe–9S–1Mo clusters are on the picosecond time scale, although the dynamics of the MoFe protein is a mixture of the dynamics of the latter two clusters. The lifetimes of the 2Fe–2S and 4Fe–4S clusters, however, extend to several nanoseconds. A competition between reorganization energies and the density of electronic states (thus electronic coupling between states) mediates the charge-transfer lifetimes, with the 2Fe–2S cluster of Pdx and the 4Fe–4S cluster of Fe protein lying at the optimum leading to them having significantly longer lifetimes. Their long lifetimes make them the optimal candidates for long-range electron transfer and as external photosensitizers for other photoactivated chemical reactions like solar hydrogen production. Potential electron-transfer and hole-transfer pathways that possibly facilitate these charge transfers are proposed.

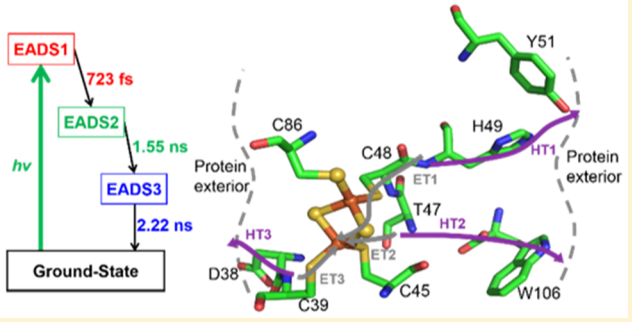

Iron–sulfur (FeS) clusters are ubiquitous in biology and not only serve as powerful electron-transfer (ET) agents and structural components for metalloenzymes but also act as catalysts in their own right.[1] They are involved in many biological processes that are essential to life on earth, photosynthesis, cellular respiration, and nitrogen fixation to name a few.[2] The complexity of FeS clusters ranges widely from simple clusters with a single iron atom like the rubredoxin protein from *Pyrococcus furiosus*[3] (*Pf*Rd) to complex multiple-iron clusters involving additional transition metal atoms like the 7Fe–9S–1Mo cofactor from molybdenum-dependent nitrogenase (Mo nitrogenase).[4] Since the importance of FeS proteins was recognized, many techniques, such as electron paramagnetic resonance spectroscopy,[5] resonance Raman,[6] and X-ray crystallography,[7] have been applied to the study of these proteins. Despite the wealth of spectroscopic, kinetic, and theoretical studies for decades, many aspects of FeS proteins are still poorly understood.

The ability to effectively and economically couple light absorption to productive outputs will be critical in the upcoming years for our developing economy. Of these processes, nitrogen fixation and hydrogen generation have garnered great interest and been extensively explored.[8,9] Recently, interest in photoinduced chemical processes involving FeS proteins has grown. For instance, FeS clusters have been reported to participate in photosensitization in living cells.[10] They also take part in photoinduced charge transfer (CT) in the purple phototroph *Rhodoferax fermentans*.[11] External photosensitizers have also been incorporated into hydrogenase and nitrogenase enzyme systems to enable photoactivated hydrogen production and nitrogen fixation.[8,9,12] Thus, FeS proteins and model compounds of FeS complexes have the potential to facilitate solar hydrogen and fuel production as external photosensitizers. While the light-induced dynamics of charge insertion in FeS complexes has been the focus of many studies,[10,11,13,14] the photodynamics induced by direct excitation of these important complexes is largely unknown. The directly excited photodynamics is important because it provides essential information about their photochemical

Received: November 15, 2017
Revised: January 4, 2018
Published: January 5, 2018

DOI: 10.1021/acs.biochem.7b01159
Biochemistry 2018, 57, 978–990

properties and how to better utilize these complexes in light-induced CT processes.

Rubredoxins are small, redox-active proteins that contain one iron atom that is coordinated in a tetrahedral geometry to the sulfur atoms of four cysteinyl residues (Figure 1A). They are

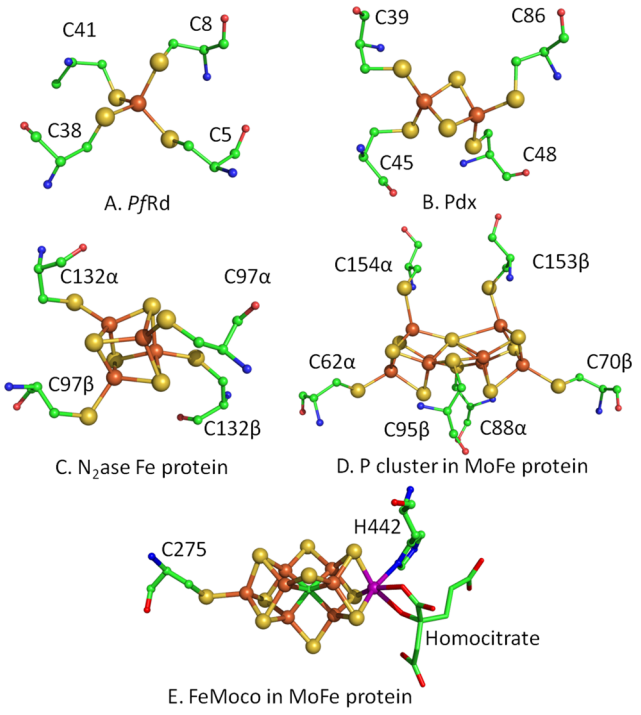

Figure 1. Active site structures of (A) *Pf*Rd, (B) Pdx, (C) nitrogenase Fe protein, (D) the 8Fe−7S P-cluster in nitrogenase MoFe protein, and (E) the 7Fe−9S−1Mo cofactor (FeMoco) in nitrogenase MoFe protein. Color coding: brick for Fe, yellow for S, green for C, blue for N, red for O, and purple for Mo. PDB entries 1BRF (*Pf*Rd), 1PUT (Pdx), 1FP6 (nitrogenase Fe protein), and 3MIN (nitrogenase MoFe protein, P cluster and FeMoco).

the smallest FeS ET proteins with typically 45−55 amino acids and are found in several anaerobic bacteria.[15] Their roles differ from organism to organism, involving electron transfer in acetogenesis[16] and reduction of nitrate,[17] alkane oxidation,[18] and superoxide reduction.[19] The rubredoxin from the hyperthermophilic archaeon *P. furiosus* (*Pf*Rd) is extremely stable, with an unfolding rate of $\sim 10^{-6}$ s^{-1} at 100 °C.[20] It has been a model for studying thermal stability of hyperthermophilic proteins. Its crystal structure has been determined by both X-ray diffraction and nuclear magnetic resonance spectroscopy (Figure 1A).[3] In this study, the CT dynamics of *Pf*Rd is compared to the dynamics of other proteins that contain multinuclear iron clusters to investigate the cluster dependence of their electronic relaxation dynamics.

The 2Fe−2S ferredoxins are small FeS proteins with 90−130 amino acids and contain a single $Fe_2S_2(S\text{-}Cys)_4$ redox center. Most 2Fe−2S ferredoxins are ET proteins, among which the putidaredoxin (Pdx) from *Pseudomonas putida* is one of the most studied. Previously, we reported the ultrafast CT dynamics in the 2Fe−2S complex of *Rhodobacter capsulatus* ferredoxin VI (Rc6).[21] Here, we extend our study to Pdx and compare it with other FeS proteins. Pdx serves as a one-electron mediator from NADH-dependent putidaredoxin reductase (Pdr) to oxygenase cytochrome P450cam in the three-component camphor hydroxylase system.[22] X-ray crystal structures of both Rc6 and Pdx (Figure 1B)[7,23] exhibit almost the same active site structures (Figure S6). Protein BLAST[24] performed on both proteins (PDB entries 1E9M for Rc6 and 1PUT for Pdx) shows that these two proteins are 41% identical and 66% similar, with an expectation value of 4×10^{-33}, which all indicate that these two proteins are highly similar to each other.

The 4Fe−4S clusters are important ET agents in ferredoxins,[25] high-potential proteins (HiPIPs),[11] nitrogenases,[26] and hydrogenases.[27] In these proteins, the cubane 4Fe−4S unit is usually coordinated by four cysteines. The oxidation states of the 4Fe−4S clusters in ferredoxins and nitrogenase iron proteins usually cycle between $[4Fe\text{−}4S]^{+}$ and $[4Fe\text{−}4S]^{2+}$, with their reduction potentials typically ranging from −700 to −300 mV.[28] In this study, the electronic relaxation dynamics of the 4Fe−4S cluster in the nitrogenase iron protein is compared to those of other FeS clusters, including the 8Fe−7S and 7Fe−9S−1Mo clusters also used by nitrogenase. Nitrogenase is the enzyme that catalyzes the conversion of dinitrogen in the air to ammonia in biological nitrogen fixation processes. It is able to break the dinitrogen triple bond at ambient temperature and atmospheric pressure and constitutes ∼50% of the global nitrogen fixation annually. However, despite nitrogenase being studied for more than 50 years, aspects of its catalytic mechanism remain poorly understood. Even which atom on the nitrogenase active site to which the dinitrogen molecule initially binds is debated.[26]

Among the different types of nitrogenases, the Mo-nitrogenase is the most common. It consists of two component proteins: the Fe protein that contains a 4Fe−4S cluster (Figure 1C) and the MoFe protein that contains an 8Fe−7S P-cluster (Figure 1D) and a 7Fe−9S−1Mo cofactor [FeMoco (Figure 1E)]. During nitrogenase turnover, electrons are transferred from the Fe protein 4Fe−4S cluster to the P-cluster of the MoFe protein and then to the FeMoco, where substrates are reduced (Figure 2). Photolysis studies of CO-inhibited

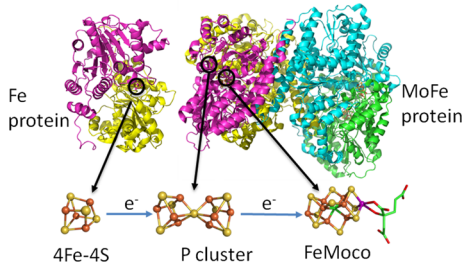

Figure 2. Electron-transfer chain in nitrogenase. PDB entries 1FP6 (nitrogenase Fe protein) and 3MIN (nitrogenase MoFe protein).

nitrogenase identified several ligand binding schemes that might be important for nitrogen turnover.[29,30] Recently, King et al. successfully incorporated an external photosensitizer to direct photoactivated ET from artificial external nanorods to the MoFe protein to facilitate nitrogen fixation.[9] However, the photodynamics inducing CT reactions of nitrogenase Fe and MoFe proteins has never been studied in detail. The knowledge of the photochemistry of the FeS clusters in Fe and MoFe proteins is helpful in the design of photoinduced nitrogenase mutants and nitrogen fixation devices. It will also aid in understanding of the photolability of ligand-bound nitrogenase, from which information about dinitrogen binding on the FeMoco can be inferred.

DOI: 10.1021/acs.biochem.7b01159
Biochemistry 2018, 57, 978−990

Recently, we reported the ultrafast electronic dynamics of the 2Fe−2S Rc6 characterized using ultrafast transient absorption (TA) spectroscopy.[21] In this paper, we extend the study on Rc6 to the FeS proteins mentioned above that contain one-Fe, two-Fe, four-Fe, seven-Fe, and eight-Fe clusters using ultrafast TA spectroscopy. TA spectroscopy directly measures the excited-state population evolution, electron transfer, intersystem crossing, etc. We aim to characterize and ultimately direct critical CT dynamics in these systems. The information about ultrafast electronic dynamics in these FeS complexes will provide useful information about the utilization of these complexes in photoinduced ET or photosensitization processes, as well as in the design of model complexes that can be used for these purposes.

MATERIALS AND METHODS

Protein Purification and Sample Preparation. *PfRd.* Recombinant *Pf*Rd (N-met form) was purified as described by Jenney and Adams,[15] except that the protein was expressed from a pET24d-derived plasmid (pETPfRd1). Plasmid pET24d was digested with *Nco*I and *Bam*HI. The rubredoxin-encoding gene (PF1282) was amplified by polymerase chain reaction from *P. furiosus* genomic DNA with NcoI and BamHI sites added at the N- and C-terminii, respectively, and cloned in frame with the translation start site of pET24d, resulting in plasmid pETPfRd1. The protein was concentrated in 50 mM Tris (pH 8.0) and 400 mM NaCl to 52 mg/mL for shipping and flash-frozen in liquid nitrogen for storage.

Pdx. The pET-Pdx plasmid was constructed by the pET vector with Pdx as the insert.[23] It was transformed into BL21 (DE3) and grown in a 17 mm × 100 mm culture tube in 6 mL of LB broth (Luria−Bertani broth) and 100 mg/mL ampicillin for 8 h at 37 °C. The cultures were then transferred to 4 × 1 L of TB (Terrific Broth) containing 100 mg/mL ampicillin. After growing at 37 °C for 12 h, cultures were induced with 0.4 mM isopropyl β-D-1-thiogalactopyranoside, and the temperature was decreased to 30 °C for 24 h. Cells were resuspended in 100 mL of 50 mM potassium phosphate (pH 7.5) before being lysed with a French press. After centrifugation to remove the cell debris, the lysate was applied to a DEAE anion exchange column (DEAE Sepharose Fast Flow, GE Healthcare), eluted with a salt gradient from 30 to 270 mM KCl in 840 mL, and fractions with an A_{412}/A_{280} ratio of >0.1 were concentrated and loaded onto a 1.8 L Sephacryl S-200 size exclusion column. The fractions with an A_{412}/A_{280} ratio of >0.48 were collected for later experiments. The Pdx protein was studied in its oxidized form.

Nitrogenase MoFe and Fe Proteins. All reagents were purchased from Sigma-Aldrich (St. Louis, MO) or Fisher Scientific (Fair Lawn, NJ) unless otherwise stated and used without further purification. *Azotobacter vinelandii* strain DJ995 (wild-type) was grown, and the corresponding nitrogenase wild-type MoFe proteins having a seven-His tag addition near the C-terminal end of the α-subunit was expressed and purified as previously described.[31] The Fe protein does not have a poly-His tag and was purified from wild-type *A. vinelandii* cells using previously published methods.[30] The protein concentration was determined by the Biuret assay using bovine serum albumin as a standard. The proton reduction (2100 nmol mg^{-1} min^{-1}) and acetylene reduction (2010 nmol mg^{-1} min^{-1}) enzymatic activity for the purified wild-type MoFe protein was determined using Fe protein as an immediate electron donor at a MoFe:Fe ratio of 1:20 (0.1 mg of MoFe protein and 0.5 mg of Fe protein) using an activity assay protocol described previously.[32] All handling of proteins and buffers was performed in septum-sealed serum vials under an argon atmosphere or on a Schlenk vacuum line.

Ultrafast Spectroscopy. The ultrafast TA system used for this study has been described previously.[33] An amplified Ti:sapphire laser system (Spectra Physics Spitfire Pro and Tsunami) generated 1 kHz repetition rate pulses at an 800 nm wavelength and a 2.5 mJ energy, with a full width at half-maximum of 40 fs. The laser beam was split into three separate paths for the generation of excitation (pump) and probe pulses. The 400 nm excitation pulses used for exciting *Pf*Rd, nitrogenase Fe protein, and nitrogenase MoFe protein were produced through second-harmonic generation (SHG) by focusing a part of the 800 nm light into a β-barium borate (BBO) crystal. The 490 nm excitation wavelength was selected for Pdx to simultaneously excite the CT transitions to iron from the opposite cysteine sulfur, the nearby cysteine sulfur, and the bridging sulfide of the 2Fe−2S cluster.[34] The 490 nm excitation pulses were generated with a home-built, noncolinear optical parametric amplifier (NOPA) that was pumped by the SHG of the 800 nm beam in another BBO crystal and seeded by a white light supercontinuum produced in a thin plate made of yttrium aluminum garnet (YAG). Another femtosecond white light continuum (350−715 nm) was generated by focusing a portion of the fundamental 800 nm pulse (~500 nJ) into a slowly translating 2 mm CaF_2 crystal for broadband probing. The angle between the polarization of the excitation and probe pulses was set at 54.7° (magic angle) with respect to each other to eliminate anisotropic effects associated with rotational dynamics. After passing through the sample, the probe light was dispersed by an imaging spectrograph (Oriel MS 127i) to a 256-pixel photodiode array (Hamamatsu S3901 and C7884). The excitation pulses were chopped at 500 Hz so that difference spectra between the excited and unexcited samples can be collected. The time delay (−10 ps to 7.5 ns) between the excitation and probe pulses was controlled by mechanically delaying the probe pulses using a computer-controlled linear motor stage (Newport IMS 600). The instrumental response for the experiment was ~150 fs.

The *Pf*Rd and Pdx samples were continuously passed through a 2 mm path length quartz cuvette using a peristaltic pump (Watson Marlow 401U/D) to ensure replenishment of new samples between successive laser shots (1 ms). The nitrogenase Fe protein and MoFe protein samples were loaded into 1 mm path length quartz cuvettes (Spectrocell Inc., R-4001-T) inside a glovebox with <2 ppm oxygen and the cuvettes tightly capped by applying vacuum grease on the threads. The cuvettes were then brought out of the glovebox and immediately sealed with low-temperature wax around the caps to further eliminate the possibility of oxygen entering the cuvettes. Two high-speed motorized actuators (Newport LTA-HS, controlled by a Newport ESP 300 motion controller) were used to translate the sample cuvettes (3 Hz, 1 cm translation distance on both *x* and *y* axes) across the laser beam[35] to avoid excessive exposure of the samples to multiple laser shots. The absorbance of all four samples was set between 0.15 and 0.7 OD unit at their respective excitation wavelength. Ultraviolet−visible absorption spectra were measured before and after the laser experiments, and no significant change to the samples was observed.

DOI: 10.1021/acs.biochem.7b01159
Biochemistry 2018, 57, 978−990

RESULTS

The steady-state absorption spectra together with the excitation laser spectra for all four proteins are shown in Figure 3. The

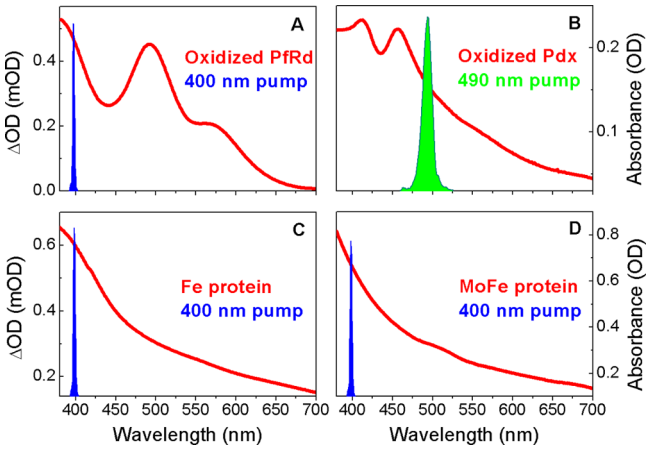

Figure 3. Static absorption spectra of (A) oxidized *Pf*Rd, (B) oxidized Pdx, (C) nitrogenase Fe protein, and (D) nitrogenase MoFe protein, together with the respective pump/excitation laser spectra.

spectra of *Pf*Rd and Pdx are typical of oxidized rubredoxin[3] and 2Fe−2S ferredoxins, respectively.[23] While the oxidized Pdx exhibits no clearly resolved absorption bands in the longer wavelength region [>465 nm (Figure 3B)], there are multiple CT transition bands of different characters buried in that region as predicted with quantum calculations by Noodleman[34] and Sharma.[36] Therefore, the pump laser at 490 nm will simultaneously excite multiple CT transitions. The spectra of both nitrogenase Fe protein and MoFe protein are relatively featureless, with absorption decreasing monotonically from the near-ultraviolet region to longer wavelengths. This indicates sample integrity during sample preparation because for both proteins distinctive features appear upon their exposure to oxygen.[37,38] Specifically, a shoulder at ∼435 nm will appear in the steady-state absorption spectrum of MoFe protein,[37] while for the Fe protein, absorption will increase in the region from 400 to 650 nm.[38] Steady-state absorption spectra taken for all four proteins after the TA experiments showed no change in the spectra and confirm that sample integrity was preserved during the ultrafast TA experiments. For the Fe protein, the steady-state spectrum displays the characteristic feature of an oxidized $[4Fe\text{-}4S]^{2+}$ cluster because upon reduction the absorption in the 350−700 nm range will decrease (Figure S8).[39]

The TA spectra at select times and kinetics at select wavelengths of *Pf*Rd are compared in Figure 4. Immediately following laser excitation, the TA spectra in the <610 nm wavelength range largely resemble the steady-state difference spectrum of reduced minus oxidized *Pf*Rd (Figure 9A), which suggests a transient reduction of the active site metal cluster induced by laser-induced LMCT. A broad positive excited-state absorption (ESA) band at ∼650 nm forms within 200 fs of laser excitation. After that, the ground-state bleach (GSB) band at ∼493 nm and the ESA band at ∼625 nm decay slowly with similar rates (Figure S7) and persist beyond 60 ps, which indicates they may represent the same intermediate species or two species that are in equilibrium. The 675 nm band decays faster than the 625 nm band does (Figure S7), indicating a different species. The two positive bands at ∼430 and ∼540 nm

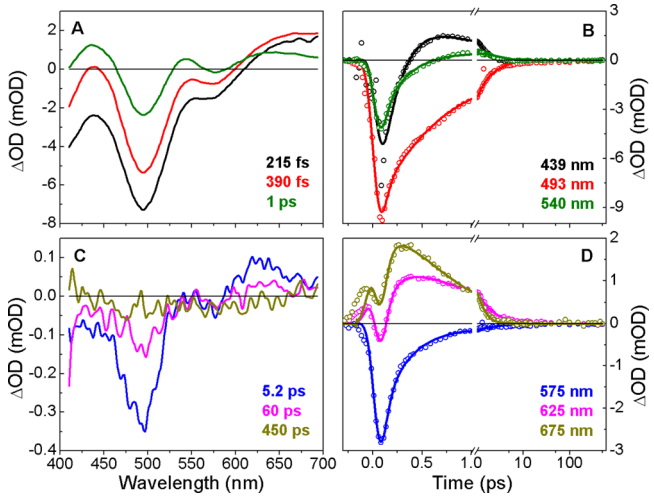

Figure 4. TA spectra of *Pf*Rd (1Fe−4S site) at select probe times (A and C), together with kinetics at select wavelengths (B and D). The empty circles represent the fits to the TA data using a five-compartment sequential model. Dispersion at different wavelengths has been adjusted to bring the beginning of the kinetics at the same time zero. The data after 1 ps are on a log time scale. Excitation at 400 nm.

form transiently (within 1 ps) and then decay within 5 ps. The TA spectra and kinetics for Pdx are shown in Figure 5. It shows

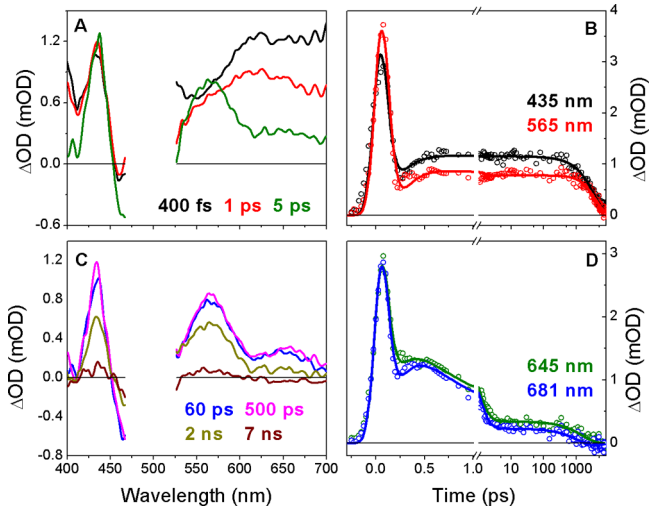

Figure 5. TA spectra of Pdx (2Fe−2S cluster) at select probe times (A and C), together with kinetics at select wavelengths (B and D). The data perturbed by the scattering of the 490 nm excitation light have been removed from the spectra. The empty circles represent the fits to the TA data using a four-compartment sequential model. Dispersion at different wavelengths has been adjusted to bring the beginning of the kinetics at the same time zero. The data after 1 ps are on a log time scale. Excitation at 490 nm.

essentially the same spectral features and kinetics as Rc6,[21] except that the early kinetics (before 200 fs) is obscured by cross phase modulation[40,41] (CPM) artifacts and stimulated Raman effects of water in the buffer solution,[42] manifested by the sharp rising and decaying phase in the early kinetics. This shows that the two 2Fe−2S ferredoxins share similar excited-state dynamics probably because they share highly similar active site structure (Figure S6; 41% identical and 66% similar with an expectation value of 4×10^{-33}).

DOI: 10.1021/acs.biochem.7b01159
Biochemistry 2018, 57, 978−990

The spectral features of *Pf*Rd are similar to those of the Pdx and Rc6, exhibiting positive ESA bands at ~430, ~540, and ~650 nm and a GSB band at ~490 nm. However, the ESA bands at 430 and 540 nm are short-lived compared to those of Pdx and Rc6. The kinetics of *Pf*Rd is very different from that of Pdx and Rc6. While the kinetics of *Pf*Rd lasts for only a few tens of picoseconds, that of Pdx and Rc6[21] persists for up to 7.2 ns.

Both nitrogenase Fe protein (Figure 6A,C) and MoFe protein (Figure 7A,C) show transient spectral features very distinct from that of *Pf*Rd (Figure 4A,C) and Pdx (Figure 5A,C), with no obvious GSB band in the 410−700 nm probing window. Although both nitrogenase Fe and MoFe proteins share somewhat similar TA spectral features, there are differences, as well. The TA spectra of the Fe protein clearly show three bands with different kinetics: (a) the short-lived positive band at ~575 nm that decays within 500 fs, (b) the positive band at ~440 nm that persists for up to 10 ps, and (c) a positive band at ~650 nm that persists for up to 7.2 ns. This suggests that there are at least three different populations in the Fe protein electronic relaxation kinetics. However, the TA spectra of the MoFe protein suggest mainly two obviously distinct bands and/or species: one at ~650 nm and the other at ~475 nm, with the 650 nm band decaying faster than the 475 nm band.

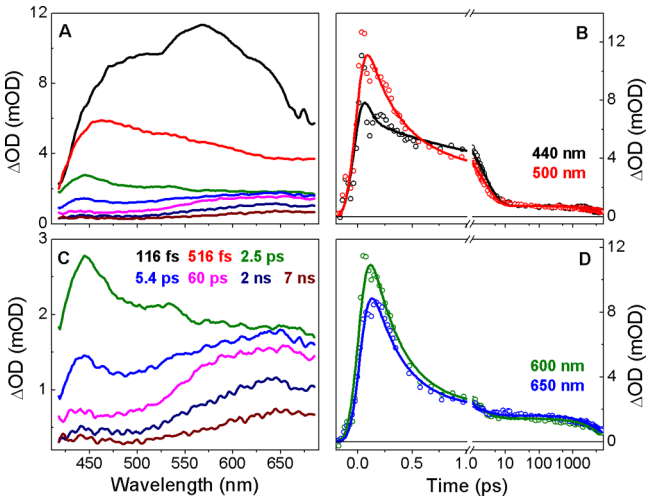

Figure 6. TA spectra of nitrogenase Fe protein (4Fe−4S cluster) at select probe times (A and C), together with kinetics at select wavelengths (B and D). The empty circles represent the fits to the TA data using a four-compartment sequential model. Dispersion at different wavelengths has been adjusted to bring the beginning of the kinetics at the same time zero. The data after 1 ps are on a log time scale. Excitation at 400 nm.

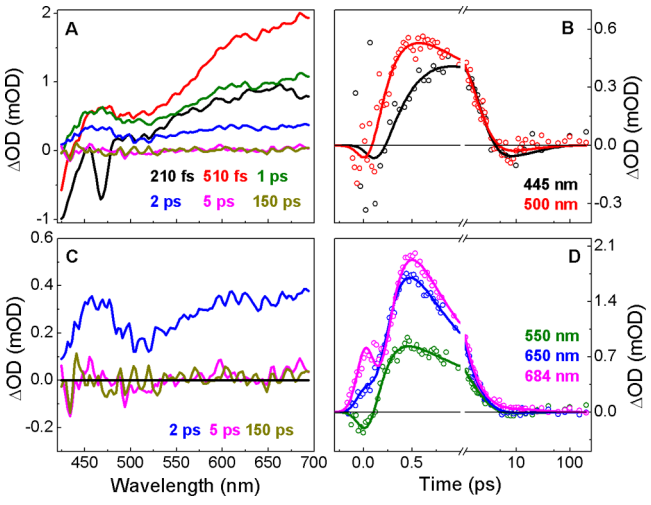

Figure 7. TA spectra of nitrogenase MoFe protein (7Fe−9S−1Mo cluster) at select probe times (A and C), together with kinetics at select wavelengths (B and D). The empty circles represent the fits to the TA data using a five-compartment sequential model. Dispersion at different wavelengths has been adjusted to bring the beginning of the kinetics at the same time zero. The data after 1 ps are on a log time scale. Excitation at 400 nm.

The electronic relaxation kinetics of the nitrogenase Fe (Figure 6B,D) and MoFe (Figure 7B,D) proteins display the most striking differences. The Fe protein transient kinetics persists beyond 7.2 ns and is slightly longer than that of Pdx, whereas the transient difference spectra of the MoFe protein decay to zero within a few tens of picoseconds and more closely resemble those of *Pf*Rd (Figure 4). For the Fe protein, the positive band on the blue side (~440 nm) decays faster than the positive band on the red side (~650 nm) of the spectra, whereas for the MoFe protein, the positive band on the blue side (~450 nm) seems to decay slightly slower than the band at the red side (~650 nm), at least on a time scale of 2 ps.

Global Analysis. We adopt a multicompartment global analysis method to simulate the data and try to unravel the underlying spectral species and their corresponding kinetics. The global analysis methodology has been described in detail previously.[43,44] To summarize, the TA data are decomposed into a set of distinct species or populations with time-independent spectra and time-dependent populations (i.e., population evolution profiles) according to a postulated model. This can be implemented numerically by fitting the data to a system of linear first-order differential eqs (eq 1):

$$\frac{dn_i}{dt} = A_i I(t) + \sum_{i,j} K_{ij} n_i \qquad (1)$$

where n_i represents the ith species or population with a time-independent spectrum, A_i represents the initial occupancy of the ith species, $I(t)$ is the excitation pulse temporal profile, and K is the matrix that describes the connectivity scheme between the underlying spectral species or populations in the postulated model, with K_{ij} being the time constant of evolution from the ith population to the jth population.

There are different global analysis models depending on the postulated connectivity schemes. One that is widely used for the fit of photodynamics is called the sequential model, where the populations are assumed to evolve from an initial population/species consecutively to the subsequent ones (A → B → C → ...). The extracted difference spectra using the sequential model are thus termed evolution-associated difference spectra (EADS). When the postulated model accurately describes the underlying photodynamics, the extracted difference spectra are also called species-associated difference spectra (SADS) and represent the true difference spectra of the constituent species in the system of interest. Otherwise, the extracted spectra do not represent the true spectra of the underlying species but are linear combinations of the true SADS. Nevertheless, EADS analysis provides useful information

DOI: 10.1021/acs.biochem.7b01159
Biochemistry 2018, 57, 978−990

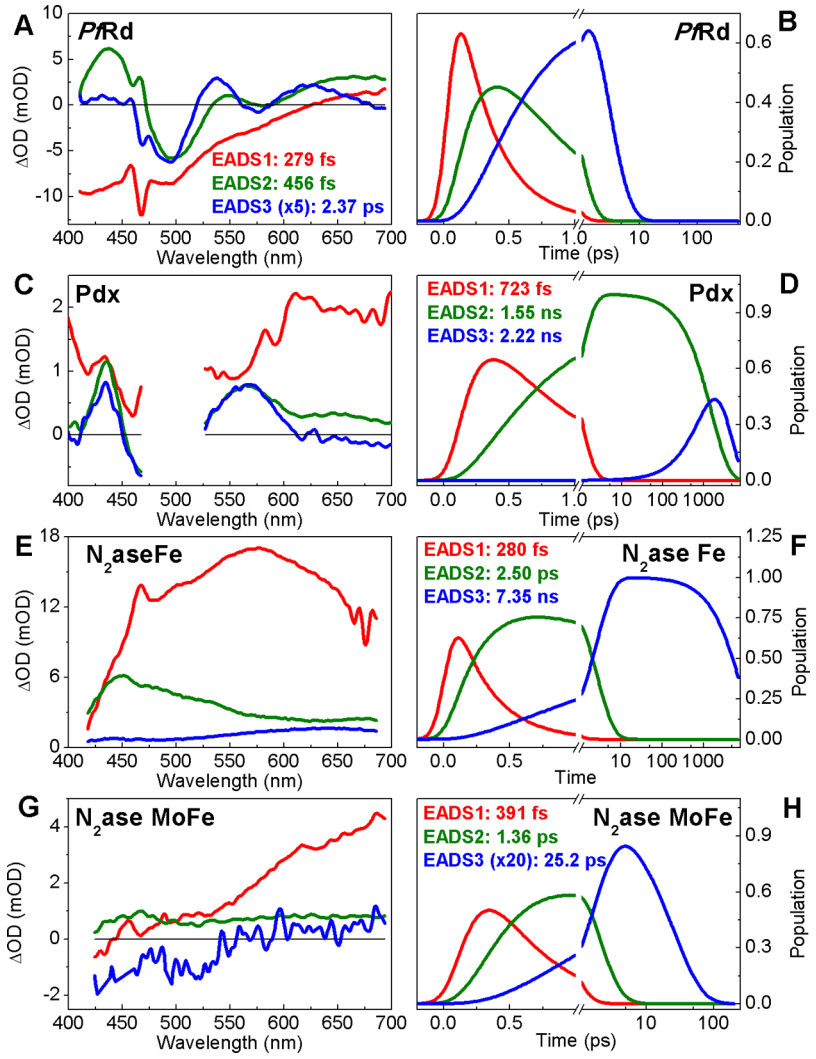

Figure 8. (A and B) Extracted EADS1−3 and corresponding population profile, respectively, for the fit of the sequential model in Figure S2 to the TA data of *Pf*Rd (Figure 4). EADS3 was scaled up 5-fold. Short-lived components used to fit the cross phase modulation (CPM) and water Raman signals[42] are shown in Figure S3. (C and D) Extracted EADS and corresponding population profile, respectively, for the fit of the sequential model in Figure S3 to the TA data of Pdx (Figure 5). Short-lived components used to fit the CPM artifact and water Raman signals are shown in Figure S3. (E and F) Extracted EADS and corresponding population profile, respectively, for the fit of the sequential model in Figure S4 to the TA data of nitrogenase (N_2ase) Fe protein (Figure 6). The short-lived component used to fit the CPM and water Raman signals is shown in Figure S4. (G and H) Extracted EADS and corresponding polulation profile, respectively, for the fit of the sequential model in Figure S5 to the TA data of N_2ase MoFe protein (Figure 7). The EADS3 was scaled up 20-fold. The short-lived components used to fit the CPM and water Raman signals are shown in Figure S5. The population profiles after 1 ps are on a log time scale.

to help unravel the underlying spectral evolution and associated directly observed time scales. It also provides insights for the construction of proper target models, although none were attempted here. Sequential model analysis of the ultrafast transient dynamics of the 2Fe−2S cluster in Rc6 successfully revealed multiple states evolving from higher excited states to lower ones.[21] Considering that the four proteins that are surveyed in this paper all contain FeS clusters, sequential model analyses suffice in describing the ultrafast electronic dynamics in these proteins, as well.

As mentioned above, direct observation of the TA data suggests that there are at least two different species in the kinetics of *Pf*Rd and MoFe protein, and at least three intermediate species in the Pdx and Fe protein data. The sequential analyses performed on the four proteins (Figure 8) used at least three compartments (Figure 8) and fit their respective TA data well (panels B and D of Figures 3−6). One obvious observation from the sequential analyses is that the EADS for all the four proteins share similar features with the TA spectra of each protein. For example, EADS2 of *Pf*Rd (Figure 8A) is similar to the TA spectrum of *Pf*Rd at 1 ps (Figure 4A), while all three EADS for Pdx (Figure 8C) resemble its TA spectra (Figure 5). The same is true with nitrogenase Fe and MoFe proteins. While the EADS for *Pf*Rd and Pdx (Figure 8A,C) may not be so obvious to observe from the raw TA data (Figures 4 and 5), the EADS of nitrogenase Fe and MoFe proteins (Figure 8E,G) can be easily identified even by merely looking at the raw transient data (Figures 6 and 7) and are thus closer to the true underlying photodynamics. Specifically, from the raw TA data of the nitrogenase Fe protein, it can be easily perceived that there is a band at ∼575 nm that forms instantaneously upon laser excitation and decays within 1 ps, leaving two positive bands at ∼450 and ∼650 nm that decay on a longer time scale, with the 650 nm one

DOI: 10.1021/acs.biochem.7b01159
Biochemistry 2018, 57, 978−990

persisting all the way to the end. For the MoFe protein, it is not difficult to identify the two positive bands at ~460 and ~650 nm, with the 650 nm band decaying faster than the 460 nm one. The third EADS in the MoFe EADS analysis is not very obvious to observe directly from the raw data. However, its presence is essential for the fit of the "dip" around 5 ps in the transient kinetics at 445 and 500 nm and thus reveals that there is a relatively long lifetime (~25.2 ps) and weak population present in the kinetics. The "ripples" at ~460 nm in EADS1 and EADS2 of *Pf*Rd probably arise from the water Raman peak.[42] It exists within only the first 200 fs, is not interesting or relevant in this study, and thus can be ignored.

The EADS for Pdx are nearly identical to the EADS previously reported for Rc6.[21] The only difference is that only three EADS are presented here for Pdx because a shorter-lived EADS (EADS3 in Figure S3) is obscured by the strong CPM artifacts[40,41] and stimulated Raman signal of water,[42] and it is difficult to extract useful information about the short-lived species from the data. Its lifetime (143 fs) is also slightly shorter than the instrumental response and thus not accurate. The details of the complete EADS analysis of Pdx with the short-lived EADS are presented in Figure S3.

DISCUSSION

In the following sections, the CT dynamics in *Pf*Rd, Pdx, and nitrogenase Fe and MoFe proteins are first discussed individually, and then their dynamics are compared to try to unravel the factors that mediate their different dynamics.

***P. furiosus* Rubredoxin.** *Pf*Rd is the simplest form of FeS protein with a mononuclear iron center coordinated with four cysteinyl sulfurs. The electronic dynamics observed in *Pf*Rd in this study is consistent with the extensive studies conducted by Kennepohl and Solomon on the electronic structure contributions to ET in 1Fe−4S clusters from *Desulfovibrio vulgaris* rubredoxin (*Dv*Rd) and in model complexes with an FeX_4 cluster (where X can be a chloride or cysteinate thiolate).[45−47] They used a series of experimental and theoretical methods, including photoelectron spectroscopy, density functional methods, and model compound studies, to investigate the effect of electronic relaxation on ET, the reduction potential of 1Fe−4S clusters, and the kinetics of ET in 1Fe−4S proteins.

This study of *Pf*Rd reveals three different populations involved in the photodynamics with lifetimes of 279 fs, 456 fs, and 2.37 ps. The first characteristic of these lifetimes is that they are all very short, which is consistent with the experimentally observed and theoretically predicted fast ET rate in rubredoxin,[48,49] as well as the short lifetime observed in the ICVS study of *Pf*Rd.[50] Figure 9A shows that the TA spectrum of *Pf*Rd at 215 fs largely resembles the difference absorption spectrum of *Pf*Rd obtained by subtracting the oxidized spectrum from the reduced spectrum. This suggests that EADS1 (279 fs) might involve a transient "internal" reduction of the active site through LMCT induced by the excitation laser. According to Kennepohl and Solomon,[45] the electronic relaxation in 1Fe−4S sites due to an increased level of LMCT is responsible for significant stabilization of the oxidized state, which may explain the transient nature of the "internal" reduction upon laser excitation. The electronic relaxation observed in 1Fe−4S clusters was also found through density functional studies to reduce both the inner-sphere reorganization energy and the electronic coupling matrix element, with the former effect dominating.[46] The large decrease in the inner-sphere reorganization energy results in an increase in the overall ET rate by 3 orders of magnitude,[46] which explains the extremely short electronic relaxation lifetimes in *Pf*Rd observed in this study.

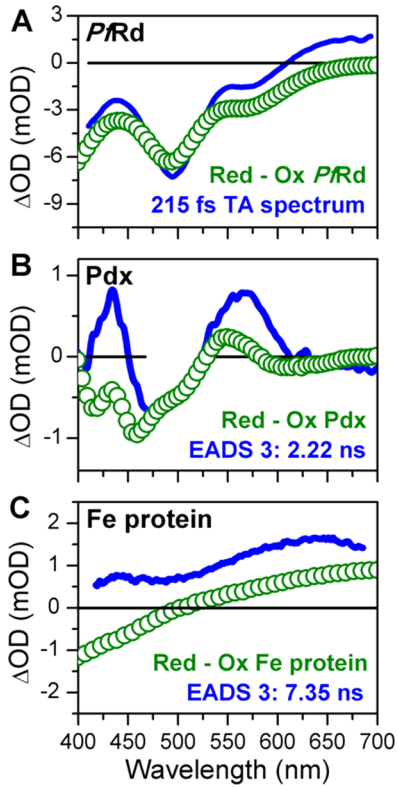

Figure 9. (A) TA spectrum of *Pf*Rd at 215 fs (blue solid curve) compared with the static difference absorption spectrum (olive empty circles) obtained by subtracting the absorption spectrum of oxidized (Ox) *Pf*Rd from that of reduced (Red) *Pf*Rd. (B) EADS3 of Pdx (blue solid curve) compared with the static difference absorption spectrum (olive empty circles) obtained by subtracting the absorption spectrum of oxidized (Ox) Pdx from that of reduced (Red) Pdx. The data perturbed by the scattering of the 490 nm excitation laser pulse have been excised from EADS3. (C) EADS3 of nitrogenase Fe protein (blue solid curve) compared with the static difference absorption spectrum (olive empty circles) obtained by subtracting the absorption spectrum of oxidized (Ox) Fe protein from that of sodium dithionite-reduced (Red) Fe protein.

The short lifetimes also suggest that there is probably no long-range photoinduced ET pathway in *Pf*Rd as was proposed in Rc6,[21] because both the short lifetimes observed in this study and the fast electron self-exchange rate observed experimentally[49] do not support long-range ET. Considering that the active site of *Pf*Rd is close to the surface of the protein, especially that Cys8 and Cys41 (in *Dv*Rd, they are Cys9 and Cys42 respectively in *Dv*Rd) are exposed to protein exterior, this makes sense because a long-range pathway is not necessary for *Pf*Rd to exchange electrons with its redox partners. However, because the level of surface exposure of the active site is very small (0.4% in *Dv*Rd), even including the regions within three σ-bonds of the active site (3.2% in *Dv*Rd),[46] it probably requires a precise docking mechanism for rubredoxin to participate in ET with redox partners or there might be some slightly longer ET pathways that extend to the surface areas slightly farther from the active site, such as those through the sulfur H-bonds of the cysteinate sulfurs to the surface amide

DOI: 10.1021/acs.biochem.7b01159
Biochemistry 2018, 57, 978−990

oxygens (approximately four σ-bonds from the active site),[46] as described below.

Despite the lack of long-range ET paths, several potential short ET pathways in *Pf*Rd have been proposed. Besides a solvent-mediated ET pathway through the proximal cysteines suggested by molecular dynamics simulations,[48] Kennepohl and Solomon proposed two major ET pathways in *Dv*Rd by employing a simple Beratan−Onuchic model to estimate the propagation of electrons through the protein matrix.[46] One is a shorter path through the β-methylenes of the surface cysteinate ligands (Cys9 and Cys42). The other is through the sulfur hydrogen bonds of the cysteinate sulfurs to the surface amide oxygens, such as those of Thr7, Val8, Gly10, Pro40, Val41, and Gly43, because the hydrogen bonds can create additional paths to the protein surface and significantly increase the surface area through which the active site can interact with its redox partners. So there are at least three potential ET pathways, with two of them being shorter (within two σ-bonds) and the other one with a slightly longer distance (up to four σ-bonds). Considering all the discussions above, the excitation laser induced a transient internal reduction of the 1Fe−4S site, probably through one or more than one of the short-range ET pathways described above, which rapidly relaxes back to the original unexcited state due to the small reorganization energy of the cluster.

***P. putida* Putidaredoxin.** Pdx is the second smallest FeS protein investigated in this study, with a 2Fe−2S cluster as the active site. Although the overall kinetics of Pdx and Fe protein both persist for up to 7 ns, Pdx has two long-lived populations with comparable lifetimes of 1.55 and 2.22 ns that potentially compete with each other, whereas the lifetimes of the three EADS of the Fe protein are more distinct with only one long-lived state. The two long-lived populations in Rc6 with a similar 2Fe−2S cluster were attributed to two different ET pathways, both of which are within three σ-bonds (within 5 Å) because the electronic decay was <8 ns.[21] The longer-lived state suggests a potentially longer-range "external" ET pathway from a surrounding amino acid to the cysteinyl sulfur of the active site and eventually to the iron atom opposite the cysteine sulfur. The other shorter-lived state possibly indicates the existence of a transient "internal" shorter-range ET from the nearby cysteinyl sulfur or the bridging sulfide to one of the iron atoms in the active site. Considering the close structural homology of Rc6 and Pdx, the two long-lived states in Pdx may also arise from similar "external" and "internal" ET pathways. The longer-lived EADS3 of Pdx resembles its reduced minus oxidized difference absorption spectrum (Figure 9B), suggesting a potential photoinduced "external" ET from a surrounding amino acid to the 2Fe−2S cluster upon laser excitation. Where the shorter-lived EADS2 is similar to EADS3, it also contains an additional positive band at ∼650 nm that is similar to that of Rc6.[21] Therefore, it is reasonable to assign the two long-lived states in Pdx to similar longer and shorter ET pathways as in Rc6 (Scheme 1, ET1 for the longer-range ET and ET2 or ET3 for the shorter-range ET).

The possible existence of the longer-range "external" ET pathway in Rc6 was further supported by the existence of hole-transfer (HT) pathways in the protein matrix to quench the electron holes created by the ET process. A similar search was made in Pdx to identify potential HT pathways. Tyrosine and tryptophan residues have been reported to participate in long-range HT in proteins because of their lower redox potential due to the change in their protonized states.[51] Therefore, the crystal

Scheme 1. Potential Electron-Transfer (ET, gray arrows) and Hole-Transfer (HT, purple arrows) Pathways in Pdx

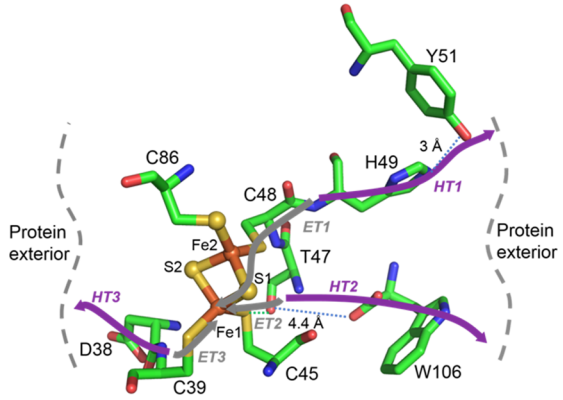

structure of Pdx was examined to identify possible tyrosine and/or tryptophan chains that are connected to the ET pathways. However, only those residues that lead to the protein exterior or the Pdx−Pdr and/or Pdx−P450cam interaction sites (e.g., near Trp106) are included in the search. Because Fe1 (Scheme 1) was reported to be preferentially reduced and favored for ET in plant-type and vertebrate-type 2Fe−2S ferredoxins,[52,53] the searches were started from Fe1.

Three major HT pathways were found in this search, corresponding to the three ET pathways shown in Scheme 1. The first one follows the same pathway that was identified in Rc6.[21] It goes through Fe1 → S1 → Cys48 → His49 → Try51 → protein exterior (ET1 and HT1 in Scheme 1). His49 is directly bound with Cys48. Its imidazole side chain is only 3 Å from the phenolic oxygen of tyrosine 51, which is solvent-exposed. The second pathway extends through Cys45 → Thr47 → Trp106 → protein exterior (HT2 in Scheme 1). This HT pathway was not identified in Rc6. However, Sevrioukova et al.[23] proposed a potential CT pathway in Pdx through the same route. It is coupled to the shorter-range ET pathway from the Cys45 sulfur to Fe1 (ET2 in Scheme 1). According to Sevrioukova et al.,[23] the threonine was included in the CT pathway for two reasons. First, Thr54 in Adx, an analogue of Thr47 in Pdx, was calculated to have the highest electron coupling value and thus is more likely to be involved in ET pathways.[54] Second, Thr47 is hydrogen bonded to the Cys45 sulfur and is partially shielded by the indole ring of Trp106, which is important in the Pdx−P450cam interaction.[55,56] The Cys45 residue has also been predicted using Harlem[56,57] to be involved in the ET pathway from the 2Fe−2S cluster of Pdx to the Fe atom of P450cam. Thus, this second ET pathway is very likely to participate in the photoinduced dynamics observed in this study. A third potential ET/HT pathway that may correspond to the shorter-lived population is from Fe1 to Cys39, Asp38, and then the protein exterior (ET3 and HT3 in Scheme 1) as was proposed by Roitberg et al. through combined theoretical and experimental studies.[58] An ET pathway from Pdr to Pdx that involves Cys39 has been predicted using Harlem.[57,59] The pair of Cys39 and Asp38 has also been predicted by Harlem to be involved in the ET from the 2Fe−2S cluster of Pdx to the heme group of P450cam.[57,59] Therefore, this pathway is also highly likely to contribute to the CT dynamics observed in the TA study.

The longer-range ET path from the opposite sulfur to iron is <5 Å; therefore, the 7 ns electronic decay time should be sufficient considering that a 25 ns ET time has been reported

DOI: 10.1021/acs.biochem.7b01159
Biochemistry 2018, 57, 978−990

for a 10 Å ET in proteins.[60] Long-range HT1 and HT2 may not occur unless they are coupled with external electron donors. The longer lifetimes as well as the cluster's proximity to the protein surface also suggest that Pdx could potentially be used as a photosensitizer for light-induced chemical reactions like hydrogen production in hydrogenase or hydrogenase model compounds.

Nitrogenase Fe Protein. The nitrogenase Fe protein contains a 4Fe−4S cluster between its two subunits and serves as the electron donor to MoFe protein during catalytic turnover. The EADS of the nitrogenase Fe protein have several distinct features. First, the EADS are all positive within the probe wavelength range, probably because the GSB band is on the blue side of the excitation laser at 400 nm and outside of the probing range of the experiment. Second, the spectral features of the three EADS are distinct and well-separated. This indicates that the three-compartment sequential model used for the fitting of the Fe protein data probably extracts and separates the underlying spectral species quite well and is likely close to the "true" model. The excitation laser promoted the sample to an excited state that subsequently evolved to two lower states, with the lowest state having a lifetime of 7 ns, and eventually decayed to the ground state. Third, although the kinetics of Pdx and Fe protein both persist for up to 7 ns, Fe protein has only one long excited state that is 2−3 times longer than that of Pdx and Rc6. Intuitively, it might be argued that the larger 4Fe−4S cluster might have a larger reorganization energy and thus leads to a slower ET rate and a longer electronic relaxation lifetime. However, theoretical calculation of the inner-sphere reorganization energies for FeS clusters with one, two, and four irons found that the reorganization energies of two-Fe (36.8 kJ/mol)[28] and four-Fe (32 kJ/mol)[28,61] clusters are very similar. Therefore, it is hard to attribute the long lifetime in the 4Fe−4S cluster to an increased reorganization energy. Considering that the 2.2 ns lifetime in 2Fe−2S clusters and the 7 ns lifetime in 4Fe−4S clusters are actually not that much different and that the cubic 4Fe−4S cluster can be viewed as six pairs of 2Fe−2S clusters, it is possible that the two different lifetimes in 2Fe−2S clusters are "smeared" into a longer lifetime in the 4Fe−4S cluster due to the coupling of electronic relaxations of the six "virtual" pairs of 2Fe−2S clusters.

Nonetheless, the long excited state may still indicate the existence of at least one CT pathway in Fe protein. Theoretical calculations performed by Aizman et al.[62] on $[Fe_4S^*_4(SCH_3)_4]^{2-}$ synthetic analogues assigned the 400−425 nm absorption band to S (3p) → Fe (3d) CT transitions. Therefore, the 400 nm excitation laser pulse promotes mostly CT transitions from the cysteinyl sulfurs to the iron atoms. Comparison of EADS3 with the reduced minus oxidized difference absorption spectrum of the Fe protein (Figure 9C) reveals that they resemble each other qualitatively, especially in the >500 nm wavelength range. This suggests that the 400 nm pump laser is probably inducing an internal reduction of the 4Fe−4S cluster that persisted for ∼7 ns. This is similar to what was observed in Pdx and Rc6 and is consistent with the fact that the 400 nm laser mostly promotes CT from the cysteinyl sulfur to the irons. It is possible that upon laser excitation, one electron on the cysteinyl sulfur was promoted to move to the irons in the 4Fe−4S cluster, and then the electron hole of the cysteine was quenched by one or multiple HT pathways that exist in the Fe protein. This indirect long distance (>10 Å) CT mechanism in FeS proteins was suggested by Noodleman and Case as early as 1984[34,63] and was reported in Rc6.[21]

However, unlike in Rc6 and Pdx, the examination of the crystal structure of the nitrogenase Fe protein failed to identify nearby tyrosine or tryptophan chains that may participate in hole quenching processes, because the closest of these residues are >10 Å from the 4Fe−4S cluster. Considering that the ET from nitrogenase Fe protein to MoFe protein requires the proper docking of these two proteins following the conformational changes induced by MgATP binding, it is possible that new ET/HT pathways between the Fe and MoFe may form after these two proteins are properly docked. Further study of this topic will help us to understand the intermolecular ET between nitrogenase component proteins. Besides the implication of ET pathways, the long lifetime also makes 4Fe−4S clusters the optimal candidate among all the investigated FeS clusters for potential application as external photosensitizers for other photoactivated reactions.

P-Cluster and FeMoco in Nitrogenase MoFe Protein. The MoFe protein contains two metal clusters. One is the 8Fe−7S P-cluster, and the other is the 7Fe−9S−1Mo FeMoco, with the P-cluster being the electron shuttle between nitrogenase Fe protein and the FeMoco (Figure 2). The measured TA signals of the MoFe protein are therefore a mixture of the signals from both clusters. Although the EADS analysis is a mixture of two different dynamic systems, what is clear is that the dynamics in both clusters are exceedingly fast. Both clusters are also larger than the other FeS clusters investigated in this study. They also both undergo structural changes upon changes in the oxidation state.[64] This suggests that the P-cluster and the FeMoco may have a larger energy barrier for electron transfer as well as larger reorganization energies, which should have contributed to lower ET rates and longer excited-state lifetimes.

Merely judging by the reorganization energies and the trend of increased lifetime from one-Fe to four-Fe clusters, it seems to suggest that the excited-state lifetimes for the P-cluster and the FeMoco should be the longest among all of those of the FeS clusters investigated in this work. However, this was not the case. The reason, we think, is because of the ignorance of a second effect that larger cluster size and greater cluster complexity may have on the electronic states of MoFe protein. While the two clusters in the MoFe protein are much larger than the other three smaller clusters, their structures are also far more complex. Especially for the FeMoco, its trigonal prismatic structure, its greater structural changes upon redox reactions,[64] and the inclusion of a transition metal element in the cluster will all contribute to increased cluster complexity. The larger size and greater complexity of the clusters will lead to a greater electronic density of states (DOS) and thus stronger electronic coupling between states.[36] According to the Fermi golden rule,[65] a larger DOS and electronic coupling will lead to a higher transition rate between states. Simply looking at the dynamics of one-, two-, and four-Fe clusters, it is tempting to conclude that a larger cluster size increases the excited-state lifetimes and thus makes a larger cluster a better candidate for long-range ET reactions and as external photosensitizers for photoactivated chemical reactions. However, the experimental data on MoFe protein refute this proposal and suggest that the increased DOS and thus stronger electronic coupling between states need to be considered as the cluster size further increases. The fact that both clusters undergo structural changes upon redox should also be considered in future studies. Therefore, although a large cluster size may allow the P-cluster to perform sequential two-electron transfers[66] and the FeMoco to facilitate

DOI: 10.1021/acs.biochem.7b01159
Biochemistry 2018, 57, 978−990

eight-electron reduction of substrates as proposed by Lowe and Thorneley,[67] it may not favor long-range ET. Intermediate ET pathways or hopping steps between the P-cluster and FeMoco are probably needed.

The existence of two clusters in the MoFe protein also explains the presence of more than two EADS because the two clusters could be simultaneously excited to their respective excited states and subsequently relax to ground states. This suggests that a parallel model might fit the data better. However, because the electronic states of MoFe protein are highly complicated because of the existence of two complex FeS clusters as well as the multiplicity of oxidation states that the two clusters can assume, it is very difficult to correctly decompose and assign the underlying spectral species. Nevertheless, the sequential analysis presented is sufficient for extracting the number of spectral species and roughly estimated their lifetimes, which are enough for the purpose of this study.

Comparison of the Charge-Transfer Dynamics. Table 1 compares the lifetimes extracted from the sequential model analyses of the TA data of the four proteins. What is puzzling is that both *Pf*Rd and the MoFe protein exhibit lifetimes significantly shorter than those of Pdx and Fe protein. The fastest decaying system is the 1Fe−4S cluster in *Pf*Rd, which is 3 orders of magnitude faster than Pdx and Fe protein. The next fastest are the two clusters in the MoFe protein.

Table 1. Lifetimes Extracted from the Sequential EADS Analyses in Figure 8

population	*Pf*Rd	Pdx	Fe protein	MoFe protein
EADS1	279 fs	723 fs	280 fs	391 fs
EADS2	456 fs	1.55 ns	2.50 ps	1.36 ps
EADS3	2.37 ps	2.22 ns	7.35 ns	25.2 ps

The overall lifetimes of Pdx and Fe protein are both on nanosecond time scales, with that of the Fe protein being slightly longer, which cannot be simply attributed to the greater reorganization energy of the 4Fe−4S cluster (32 kJ/mol)[61] because it is actually very close to and even smaller than that of the 2Fe−2S cluster (36.8 kJ/mol).[28] As discussed above, the single long lifetime in the Fe protein might be due to the coupling of the six "virtual" pairs of 2Fe−2S clusters constituting the cubic 4Fe−4S cluster, which "smears" out the two long lifetimes in 2Fe−2S clusters. The reorganization energy of rubredoxin (∼20 kJ/mol)[28,61] is almost half of that of 2Fe−2S and 4Fe−4S clusters. Therefore, the shorter lifetime of rubredoxin might be attributed to the smaller reorganization energy as proposed by Kennepohl and Solomon et al.[46] The increasing lifetimes from one- to four-Fe clusters seem to suggest the MoFe protein should have an even longer lifetime, which turns out to be the opposite of the reality. Considering that the two clusters in the MoFe protein are considerably more complex, the fast-decaying kinetics is probably due to the greater electronic DOS in these two clusters and thus stronger electronic coupling between states. According to Sharma et al.,[36] even for clusters as simple as 2Fe−2S and 4Fe−4S clusters, there are several more magnitudes of electronic states than previously predicted. Therefore, the larger clusters in MoFe protein probably have much more electronic states congested in the lower-energy range than the simpler clusters do.

We thus postulate that the cluster size has mainly two effects on the excited-state relaxation dynamics of FeS proteins. (1) Increased cluster size in general increases the reorganization energy of the cluster and thus tends to increase the electronic-state lifetimes. This effect may explain rubredoxin's extremely short excited-state lifetime. However, the direct relationship between cluster size and reorganization energy is difficult to establish because there are too many complicating factors as evidenced in 2Fe−2S and 4Fe−4S clusters. (2) Larger cluster size and greater cluster complexity increase the DOS and electronic coupling between states, thus decreasing the excited-state lifetimes. From *Pf*Rd (1Fe−4S), Pdx (2Fe−2S), and Fe protein (4Fe−4S) to the P-cluster (8Fe−7S), the main contributing factor to increased cluster complexity is increased cluster size. However, for the P-cluster and FeMoco of nitrogenase, the more complicated overall structures, the larger structural changes upon redox reactions, and the inclusion of a transition metal also contribute to the increased cluster complexity. These all lead to a greater DOS in these two clusters.

CONCLUDING COMMENTS

The electronic relaxation dynamics slow down with an increase in cluster size from one- to four-Fe clusters and then become faster from four-Fe to seven- and eight-Fe clusters. The longer-lived CT states in 2Fe−2S clusters thus are not representative of the CT kinetics of all FeS clusters. Therefore, there is no direct relationship between cluster size and electronic relaxation dynamics in FeS clusters. The competition between the reorganization energy and DOS probably mediates their electronic relaxation lifetimes. In the efforts to construct novel materials or biofunctional proteins capable of utilizing CT properties, long-lived CT states are usually required. This suggests that 2Fe−2S or 4Fe−4S clusters, which have excited states that last much longer than the other clusters, are the optimal clusters to start with among FeS proteins. Because of the complexity of the P-cluster and the FeMoco, as well as the fact that their TA signals are a mixture of signals from both clusters, their CT properties are much more difficult to study than the smaller clusters with one to four irons. This study contributes some insight into a more complete understanding of the CT dynamics in these larger FeS clusters.

ASSOCIATED CONTENT

Supporting Information

The Supporting Information is available free of charge on the ACS Publications website at DOI: 10.1021/acs.biochem.7b01159.

Details of sequential analyses, schematic of the experimental setup, and additional information about the protein structure and absorption spectra (PDF)

AUTHOR INFORMATION

Corresponding Authors

*E-mail: dlarsen@ucdavsi.edu.
*E-mail: spjcramer@ucdavis.edu.

ORCID

David B. Goodin: 0000-0002-9196-0001
Lance C. Seefeldt: 0000-0002-6457-9504
Delmar S. Larsen: 0000-0003-4522-2689

Present Addresses

⊥S.-H.L.: Max Planck Institute for Biophysical Chemistry, Am Fassberg 11, 37077 Göttingen, Germany.

DOI: 10.1021/acs.biochem.7b01159
Biochemistry 2018, 57, 978−990

[#]N.K.: Department of Pharmacology, Case Western Reserve University, Cleveland, OH 44106.

Funding

This work was supported by grants from the National Institutes of Health to S.P.C. (GM65440), the Division of Chemical Sciences, Geosciences and Biosciences, Office of Basic Energy Sciences, U.S. Department of Energy, to M.W.W.A. (DE-FG05-95ER20175), and the National Science Foundation to D.S.L. (CHE-1413739) and S.P.C. (CHE-1308384). Nitrogenase work was supported by a grant from the Department of Energy, Office of Basic Energy Sciences, to L.C.S. (DE-SC0010687).

Notes

The authors declare no competing financial interest.

■ ACKNOWLEDGMENTS

The authors acknowledge Dr. Mikas Vengris from Light Conversion Ltd. for donating the global analysis software package. The authors thank Dr. Simon Arragain and Prof. Alexei Stuchebrukhov of the University of California at Davis for helpful discussions.

■ ABBREVIATIONS

FeS, iron−sulfur; FeMoco, iron−molybdenum cofactor; ET, electron transfer; HT, hole transfer; CT, charge transfer; *Pf*Rd, *P. furiosus* rubredoxin; *Dv*Rd, *D. vulgaris* rubredoxin; Pdx, putidaredoxin; Rc6, *R. capsulatus* ferredoxin VI; Fe protein, nitrogenase iron protein; MoFe protein, nitrogenase molybdenum−iron protein; EPR, electron paramagnetic resonance spectroscopy; NOPA, noncolinear optical parametric amplifier; TA, transient absorption; ICVS, impulsive coherent vibrational spectroscopy; BBO, β barium borate; SHG, second-harmonic generation; YAG, yttrium aluminum garnet; LMCT, ligand-to-metal charge transfer; ESA, excited-state absorption; GSB, ground-state bleaching; EADS, evolution-associated difference spectra; SADS, species-associated difference spectra; OD, optical density; CPM, cross-phase modulation; DOS, density of states; PDB, Protein Data Bank.

■ REFERENCES

(1) Meyer, J. (2008) Iron-sulfur protein folds, iron-sulfur chemistry, and evolution. *JBIC, J. Biol. Inorg. Chem. 13*, 157−170.

(2) Johnson, D. C., Dean, D. R., Smith, A. D., and Johnson, M. K. (2005) Structure, function, and formation of biological iron-sulfur clusters. *Annu. Rev. Biochem. 74*, 247−281.

(3) Bau, R., Rees, D. C., Kurtz, D. M., Jr., Scott, R. A., Huang, H. S., Adams, M. W. W., and Eidsness, M. K. (1998) Crystal structure of rubredoxin from Pyrococcus furiosus at 0.95 angstrom resolution, and the structures of N-terminal methionine and formylmethionine variants of Pf Rd. Contributions of N-terminal interactions to thermostability. *JBIC, J. Biol. Inorg. Chem. 3*, 484−493.

(4) Einsle, O., Tezcan, F. A., Andrade, S. L. A., Schmid, B., Yoshida, M., Howard, J. B., and Rees, D. C. (2002) Nitrogenase MoFe-protein at 1.16 angstrom resolution: A central ligand in the FeMo-cofactor,. *Science 297*, 1696−1700.

(5) Guigliarelli, B., and Bertrand, P. (1999) Application of EPR spectroscopy to the structural and functional study of iron-sulfur proteins. *Adv. Inorg. Chem. 47*, 421−497.

(6) Ozaki, Y., Nagayama, K., Kyogoku, Y., Hase, T., and Matsubara, H. (1983) Resonance Raman-Spectroscopic Study on the Iron Sulfur Proteins Containing [2fe-2s] Clusters. *FEBS Lett. 152*, 236−240.

(7) Sainz, G., Jakoncic, J., Sieker, L. C., Stojanoff, V., Sanishvili, N., Asso, M., Bertrand, P., Armengaud, J., and Jouanneau, Y. (2006) Structure of a [2Fe-2S] ferredoxin from Rhodobacter capsulatus likely involved in Fe-S cluster biogenesis and conformational changes observed upon reduction. *J. Biol. Inorg. Chem. 11*, 235−246.

(8) Brown, K. A., Dayal, S., Ai, X., Rumbles, G., and King, P. W. (2010) Controlled Assembly of Hydrogenase-CdTe Nanocrystal Hybrids for Solar Hydrogen Production. *J. Am. Chem. Soc. 132*, 9672−9680.

(9) Brown, K. A., Harris, D. F., Wilker, M. B., Rasmussen, A., Khadka, N., Hamby, H., Keable, S., Dukovic, G., Peters, J. W., Seefeldt, L. C., and King, P. W. (2016) Light-driven dinitrogen reduction catalyzed by a CdS:nitrogenase MoFe protein biohybrid. *Science 352*, 448−450.

(10) Kim, C. S., and Jung, J. (1992) Iron Sulfur Centers as Endogenous Blue-Light Sensitizers in Cells - a Study with an Artificial Nonheme Iron Protein. *Photochem. Photobiol. 56*, 63−68.

(11) Hochkoeppler, A., Zannoni, D., Ciurli, S., Meyer, T. E., Cusanovich, M. A., and Tollin, G. (1996) Kinetics of photo-induced electron transfer from high-potential iron-sulfur protein to the photosynthetic reaction center of the purple phototroph Rhodoferax fermentans. *Proc. Natl. Acad. Sci. U. S. A. 93*, 6998−7002.

(12) Adam, D., Bosche, L., Castaneda-Losada, L., Winkler, M., Apfel, P., and Happe, T. (2017) Sunlight-Dependent Hydrogen Production by Photosensitizer/Hydrogenase Systems. *ChemSusChem 10*, 894−902.

(13) Wang, W. G., Rauchfuss, T. B., Bertini, L., and Zampella, G. (2012) Unsensitized Photochemical Hydrogen Production Catalyzed by Diiron Hydrides. *J. Am. Chem. Soc. 134*, 4525−4528.

(14) Engstrom, G., Xiao, K. H., Yu, C. A., Yu, L., Durham, B., and Millett, F. (2002) Photoinduced electron transfer between the Rieske iron-sulfur protein and cytochrome c(1) in the Rhodobacter sphaeroides cytochrome bc(1) complex - Effects of pH, temperature, and driving force. *J. Biol. Chem. 277*, 31072−31078.

(15) Jenney, F. E., and Adams, M. W. W. (2001) Rubredoxin from Pyrococcus furiosus. *Methods Enzymol. 334*, 45−55.

(16) Hugenholtz, J., and Ljungdahl, L. G. (1990) Amino-Acid-Transport in Membrane-Vesicles of Clostridium-Thermoautotrophicum. *FEMS Microbiol. Lett. 69*, 117−121.

(17) Seki, Y., Seki, S., Satoh, M., Ikeda, A., and Ishimoto, M. (1989) Rubredoxin from Clostridium-Perfringens - Complete Amino-Acid Sequence and Participation in Nitrate Reduction. *J. Biochem. 106*, 336−341.

(18) van Beilen, J. B., Neuenschwander, M., Smits, T. H. M., Roth, C., Balada, S. B., and Witholt, B. (2002) Rubredoxins involved in alkane oxidation. *J. Bacteriol. 184*, 1722−1732.

(19) Auchere, F., Sikkink, R., Cordas, C., Raleiras, P., Tavares, P., Moura, I., and Moura, J. J. G. (2004) Overexpression and purification of Treponema pallidum rubredoxin; kinetic evidence for a superoxide-mediated electron transfer with the superoxide reductase neelaredoxin. *JBIC, J. Biol. Inorg. Chem. 9*, 839−849.

(20) Hernandez, G., Jenney, F. E., Adams, M. W. W., and LeMaster, D. M. (2000) Millisecond time scale conformational flexibility in a hyperthermophile protein at ambient temperature. *Proc. Natl. Acad. Sci. U. S. A. 97*, 3166−3170.

(21) Mao, Z., Carroll, E. C., Kim, P. W., Cramer, S. P., and Larsen, D. S. (2017) Ultrafast Charge Transfer Dynamics in the Iron-Sulfur Complex of Rhodobacter Capsulatus Ferredoxin VI. *J. Phys. Chem. Lett. 8*, 4498−4503.

(22) Katagiri, M., Ganguli, B. N., and Gunsalus, I. C. (1968) A Soluble Cytochrome P-450 Functional in Methylene Hydroxylation,. *J. Biol. Chem. 243*, 3543.

(23) Sevrioukova, I. F., Garcia, C., Li, H. Y., Bhaskar, B., and Poulos, T. L. (2003) Crystal structure of putidaredoxin, the [2Fe-2S] component of the P450cam monooxygenase system from Pseudomonas putida. *J. Mol. Biol. 333*, 377−392.

(24) Boratyn, G. M., Camacho, C., Cooper, P. S., Coulouris, G., Fong, A., Ma, N., Madden, T. L., Matten, W. T., McGinnis, S. D., Merezhuk, Y., Raytselis, Y., Sayers, E. W., Tao, T., Ye, J., and Zaretskaya, I. (2013) BLAST: a more efficient report with usability improvements. *Nucleic Acids Res. 41*, W29−W33.

(25) Dauter, Z., Wilson, K. S., Sieker, L. C., Meyer, J., and Moulis, J. M. (1997) Atomic resolution (0.94 angstrom) structure of

DOI: 10.1021/acs.biochem.7b01159
Biochemistry 2018, 57, 978−990

Clostridium acidurici ferredoxin. Detailed geometry of [4Fe-4S] clusters in a protein. *Biochemistry 36*, 16065−16073.
(26) Hoffman, B. M., Lukoyanov, D., Yang, Z. Y., Dean, D. R., and Seefeldt, L. C. (2014) Mechanism of Nitrogen Fixation by Nitrogenase: The Next Stage,. *Chem. Rev. 114*, 4041−4062.
(27) Peters, J. W., Lanzilotta, W. N., Lemon, B. J., and Seefeldt, L. C. (1998) X-ray crystal structure of the Fe-only hydrogenase (Cpl) from Clostridium pasteurianum to 1.8 angstrom resolution. *Science 282*, 1853−1858.
(28) Sigfridsson, E., Olsson, M. H. M., and Ryde, U. (2001) Inner-sphere reorganization energy of iron-sulfur clusters studied with theoretical methods. *Inorg. Chem. 40*, 2509−2519.
(29) Maskos, Z., and Hales, B. J. (2003) Photo-lability of CO bound to mo-nitrogenase from Azotobacter vinelandii. *J. Inorg. Biochem. 93*, 11−17.
(30) Yan, L. F., Dapper, C. H., George, S. J., Wang, H. X., Mitra, D., Dong, W. B., Newton, W. E., and Cramer, S. P. (2011) Photolysis of Hi-CO Nitrogenase - Observation of a Plethora of Distinct CO Species Using Infrared Spectroscopy. *Eur. J. Inorg. Chem. 2011*, 2064−2074.
(31) Christiansen, J., Goodwin, P. J., Lanzilotta, W. N., Seefeldt, L. C., and Dean, D. R. (1998) Catalytic and biophysical properties of a nitrogenase apo-MoFe protein produced by a nifB-deletion mutant of Azotobacter vinelandii. *Biochemistry 37*, 12611−12623.
(32) Christiansen, J., Cash, V. L., Seefeldt, L. C., and Dean, D. R. (2000) Isolation and characterization of an acetylene-resistant nitrogenase. *J. Biol. Chem. 275*, 11459−11464.
(33) Carroll, E. C., Compton, O. C., Madsen, D., Osterloh, F. E., and Larsen, D. S. (2008) Ultrafast carrier dynamics in exfoliated and functionalized calcium niobate nanosheets in water and methanol. *J. Phys. Chem. C 112*, 2394−2403.
(34) Noodleman, L., and Baerends, E. J. (1984) Electronic-Structure, Magnetic-Properties, Electron-Spin-Resonance, and Optical-Spectra for 2-Fe Ferredoxin Models by Lcao-X-Alpha Valence Bond Theory. *J. Am. Chem. Soc. 106*, 2316−2327.
(35) Larsen, D. S. (2002) A small volume, rapid translation cryostat insert constructed from commercial components for the detection of ultrafast optical signals. *Rev. Sci. Instrum. 73*, 1325−1328.
(36) Sharma, S., Sivalingam, K., Neese, F., and Chan, G. K. L. (2014) Low-energy spectrum of iron-sulfur clusters directly from many-particle quantum mechanics. *Nat. Chem. 6*, 927−933.
(37) Stephens, P. J., Mckenna, C. E., Smith, B. E., Nguyen, H. T., Mckenna, M. C., Thomson, A. J., Devlin, F., and Jones, J. B. (1979) Circular-Dichroism and Magnetic Circular-Dichroism of Nitrogenase Proteins. *Proc. Natl. Acad. Sci. U. S. A. 76*, 2585−2589.
(38) Shah, V. K., and Brill, W. J. (1973) Nitrogenase 0.4. Simple Method of Purification to Homogeneity of Nitrogenase Components from Azotobacter-Vinelandil. *Biochim. Biophys. Acta, Bioenerg. 305*, 445−454.
(39) Arragain, S., Garcia-Serres, R., Blondin, G., Douki, T., Clemancey, M., Latour, J. M., Forouhar, F., Neely, H., Montelione, G. T., Hunt, J. F., Mulliez, E., Fontecave, M., and Atta, M. (2010) Post-translational Modification of Ribosomal Proteins Structural and Functional Characterization of RimO from Thermotoga maritima, a Radical S-Adenosylmethionine Methylthiotransferase. *J. Biol. Chem. 285*, 5792−5801.
(40) Kovalenko, S. A., Dobryakov, A. L., Ruthmann, J., and Ernsting, N. P. (1999) Femtosecond spectroscopy of condensed phases with chirped supercontinuum probing. *Phys. Rev. A: At., Mol., Opt. Phys. 59*, 2369−2384.
(41) Ekvall, K., van der Meulen, P., Dhollande, C., Berg, L. E., Pommeret, S., Naskrecki, R., and Mialocq, J. C. (2000) Cross phase modulation artifact in liquid phase transient absorption spectroscopy. *J. Appl. Phys. 87*, 2340−2352.
(42) Lorenc, M., Ziolek, M., Naskrecki, R., Karolczak, J., Kubicki, J., and Maciejewski, A. (2002) Artifacts in femtosecond transient absorption spectroscopy. *Appl. Phys. B: Lasers Opt. 74*, 19−27.
(43) van Stokkum, I. H. M., Larsen, D. S., and van Grondelle, R. (2004) Global and target analysis of time-resolved spectra. *Biochim. Biophys. Acta, Bioenerg. 1657*, 82−104.
(44) Holzwarth, A. R. (1996) Data Analysis of Time-Resolved Measurements. In *Biophysical techniques in photosynthesis* (Amesz, J., and Hoff, A. J., Eds.) pp 75−92, Springer, Dordrecht, The Netherlands.
(45) Kennepohl, P., and Solomon, E. I. (2003) Electronic structure contributions to electron-transfer reactivity in iron-sulfur active sites: 1. Photoelectron spectroscopic determination of electronic relaxation. *Inorg. Chem. 42*, 679−688.
(46) Kennepohl, P., and Solomon, E. I. (2003) Electronic structure contributions to electron-transfer reactivity in iron-sulfur active sites: 3. Kinetics of electron transfer. *Inorg. Chem. 42*, 696−708.
(47) Kennepohl, P., and Solomon, E. I. (2003) Electronic structure contributions to electron-transfer reactivity in iron-sulfur active sites: 2. Reduction potentials. *Inorg. Chem. 42*, 689−695.
(48) Yang, Y., Beck, B. W., Shenoy, V. S., and Ichiye, T. (1993) Aqueous Solvation of a Rubredoxin Redox Site Analog - a Molecular-Dynamics Simulation. *J. Am. Chem. Soc. 115*, 7439−7444.
(49) Im, S. G., and Sykes, A. G. (1996) Kinetic studies on the redox reactions of Clostridium pasteurianum rubredoxin. *J. Chem. Soc., Dalton Trans.*, 2219−2222.
(50) Tan, M. L., Bizzarri, A. R., Xiao, Y. M., Cannistraro, S., Ichiye, T., Manzoni, C., Cerullo, G., Adams, M. W. W., Jenney, F. E., and Cramer, S. P. (2007) Observation of terahertz vibrations in Pyrococcus furiosus rubredoxin via impulsive coherent vibrational spectroscopy and nuclear resonance vibrational spectroscopy - interpretation by molecular mechanics. *J. Inorg. Biochem. 101*, 375−384.
(51) Gray, H. B., and Winkler, J. R. (2015) Hole hopping through tyrosine/tryptophan chains protects proteins from oxidative damage. *Proc. Natl. Acad. Sci. U. S. A. 112*, 10920−10925.
(52) Holden, H. M., Jacobson, B. L., Hurley, J. K., Tollin, G., Oh, B. H., Skjeldal, L., Chae, Y. K., Cheng, H., Xia, B., and Markley, J. L. (1994) Structure-Function Studies of [2fe-2s] Ferredoxins. *J. Bioenerg. Biomembr. 26*, 67−88.
(53) Dugad, L. B., Lamar, G. N., Banci, L., and Bertini, I. (1990) Identification of Localized Redox States in Plant-Type 2-Iron Ferredoxins Using the Nuclear Overhauser Effect. *Biochemistry 29*, 2263−2271.
(54) Hannemann, F., Rottmann, M., Schiffler, B., Zapp, J., and Bernhardt, R. (2001) The loop region covering the iron-sulfur cluster in bovine adrenodoxin comprises a new interaction site for redox partners. *J. Biol. Chem. 276*, 1369−1375.
(55) Stayton, P. S., and Sligar, S. G. (1991) Structural Micro-heterogeneity of a Tryptophan Residue Required for Efficient Biological Electron-Transfer between Putidaredoxin and Cyto-chrome-P-450cam. *Biochemistry 30*, 1845−1851.
(56) Kuznetsov, V. Y., Poulos, T. L., and Sevrioukova, I. F. (2006) Putidaredoxin-to-cytochrome P450cam electron transfer: Differences between the two reductive steps required for catalysis. *Biochemistry 45*, 11934−11944.
(57) Kurnikov, I. V. (2000) *HARLEM molecular modeling package*, version 1.0, Department of Chemistry, University of Pittsburgh, Pittsburgh, PA.
(58) Roitberg, A., Holden, M., Mayhew, M., Beratan, D., Kurnikov, I., and Vilker, V. (1998) Binding and electron transfer between putidaredoxin and cytochrome P450cam. Theory and experiments. *J. Am. Chem. Soc. 120*, 8927−8932.
(59) Sevrioukova, I. F., Poulos, T. L., and Churbanova, I. Y. (2010) Crystal Structure of the Putidaredoxin Reductase. Putidaredoxin Electron Transfer Complex. *J. Biol. Chem. 285*, 13616−13620.
(60) Byrdin, M., Sartor, V., Eker, A. P. M., Vos, M. H., Aubert, C., Brettel, K., and Mathis, P. (2004) Intraprotein electron transfer and proton dynamics during photoactivation of DNA photolyase from E-coli: review and new insights from an ″inverse″ deuterium isotope effect. *Biochim. Biophys. Acta, Bioenerg. 1655*, 64−70.

DOI: 10.1021/acs.biochem.7b01159
Biochemistry 2018, 57, 978−990

(61) Reynolds, J. G., Coyle, C. L., and Holm, R. H. (1980) Electron Exchange Kinetics of [Fe4s4(Sr)4]2−[Fe4s4(Sr)4]3-and [Fe4se4(Sr)-4]2−[Fe4se4(Sr)4]3-Systems - Estimates of the Intrinsic Self-Exchange Rate-Constant of 4-Fe Sites in Oxidized and Reduced Ferredoxins. *J. Am. Chem. Soc. 102*, 4350−4355.
(62) Aizman, A., and Case, D. A. (1982) Electronic-Structure Calculations on Active-Site Models for 4-Fe, 4-S Iron Sulfur Proteins. *J. Am. Chem. Soc. 104*, 3269−3279.
(63) Noodleman, L., Norman, J. G., Osborne, J. H., Aizman, A., and Case, D. A. (1985) Models for Ferredoxins - Electronic-Structures of Iron Sulfur Clusters with One, 2, and 4 Iron Atoms. *J. Am. Chem. Soc. 107*, 3418−3426.
(64) Yang, Z. Y., Danyal, K., and Seefeldt, L. C. (2011) Mechanism of Mo-Dependent Nitrogenase. *Methods Mol. Biol. 766*, 9−29.
(65) Fermi, E. (1950) *Nuclear Physics*, University of Chicago Press, Chicago.
(66) Peters, J. W., Fisher, K., Newton, W. E., and Dean, D. R. (1995) Involvement of the P Cluster in Intramolecular Electron Transfer within the Nitrogenase MoFe protein. *J. Biol. Chem. 270*, 27007−27013.
(67) Thorneley, R. N. F., and Lowe, D. (1985) Kinetics and mechanism of the nitrogenase enzyme system. In *Molybdenum Enzymes* (Spiro, T. G., Ed.) pp 221−284, Wiley, New York.

DOI: 10.1021/acs.biochem.7b01159
Biochemistry 2018, 57, 978−990